Supporting Information for

A Highly Stretchable and Robust Non-fluorinated Superhydrophobic Surface

Jie Ju[†], *Xi Yao*[†], *Xu Hou*, *Qihan Liu*, *Yu Shrike Zhang*[*] and *Ali Khademhosseini*[*]

[†]*These authors contributed equally to this work*

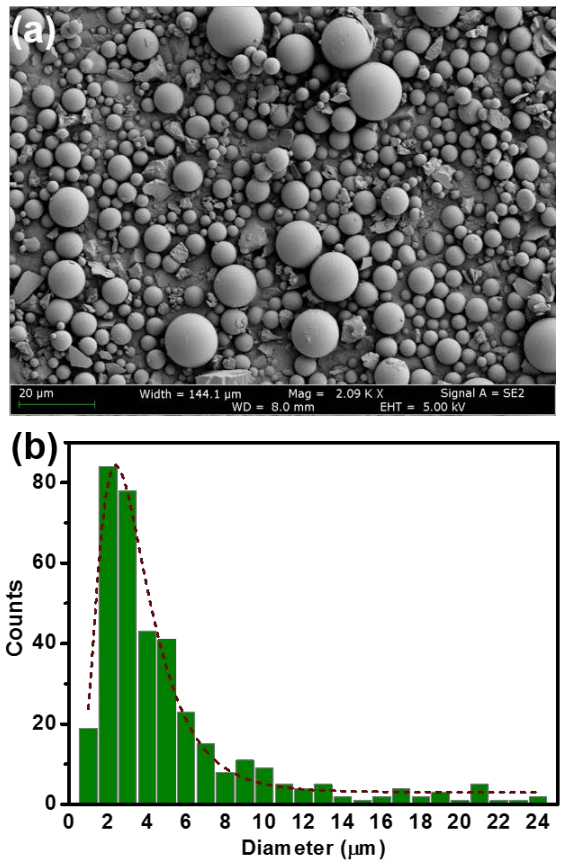

Fig. S1. Size distribution of the silica microparticles. (a) SEM image of the silica microparticles. (b) Quantification of diameter distribution of the silica microparticles, indicating the distribution from 1 µm to 24 µm with mostly falling in the range of 2-5 µm.

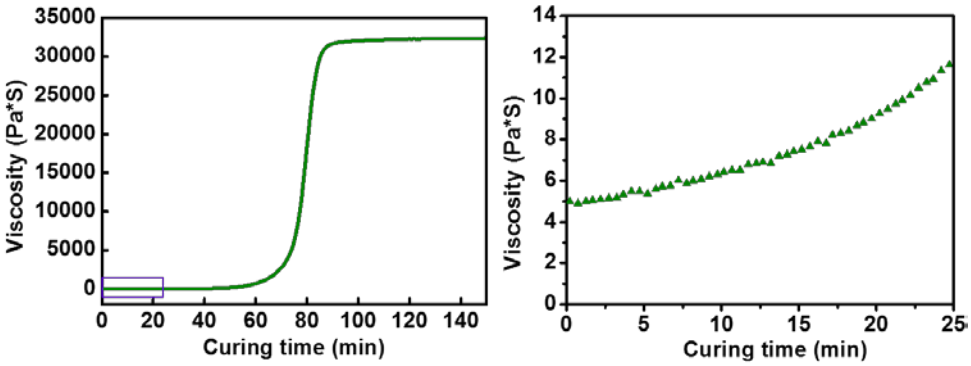

Fig. S2. Viscosity of the silicone oligomer after different curing time at room temperature. With increasing curing time, the viscosity increased slowly in the first 60 min, and then sharply from 60 min to 80 min, after which the viscosity remained constant.

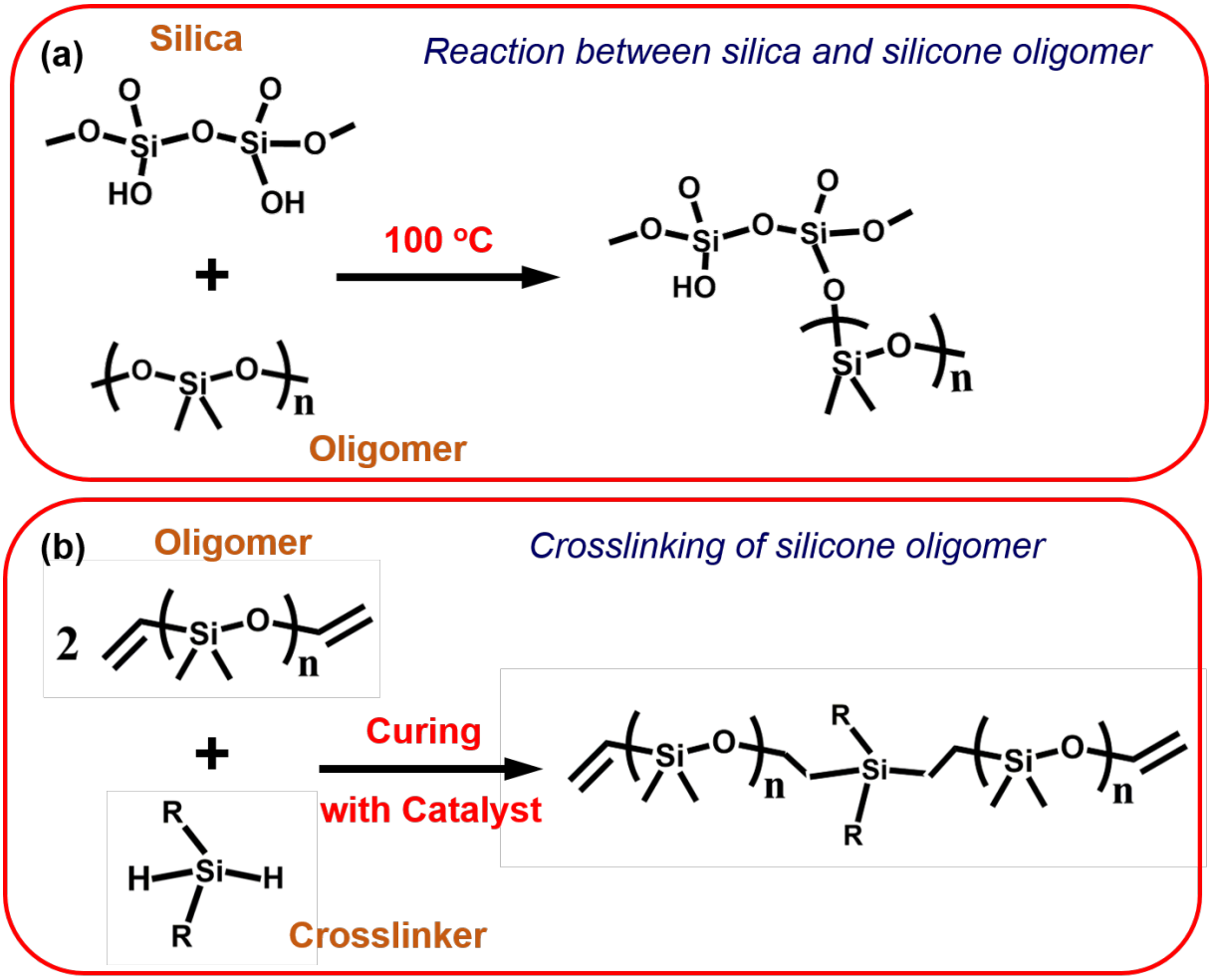

Fig. S3. Schemes showing (a) chemical reaction between silica and silicone oligomer and (b) curing of the silicone elastomer in our experiment.

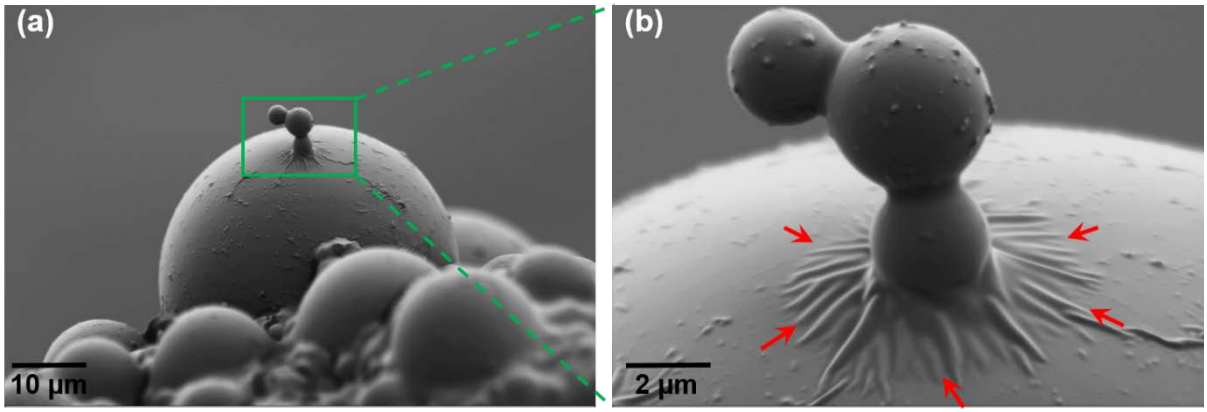

Fig. S4. SEM images of the silica microparticles wrapped by silicone elastomer. (b) is the magnified image of area highlighted with green rectangle in (a). Red arrows in (b) denote the silicone wrinkles.

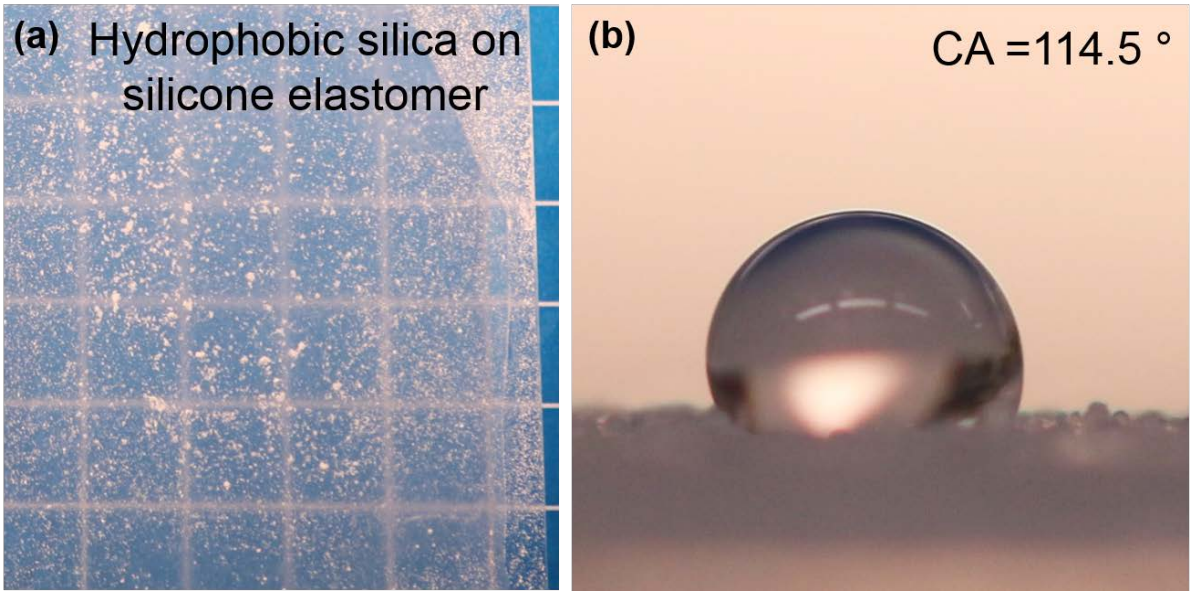

Fig. S5. Gross morphology and water contact angle of the silicone elastomer with hydrophobic silica microparticle deposition. (a) The surface shows non-uniform scattered silica microparticle islands. (b) Water contact angle of the surface.

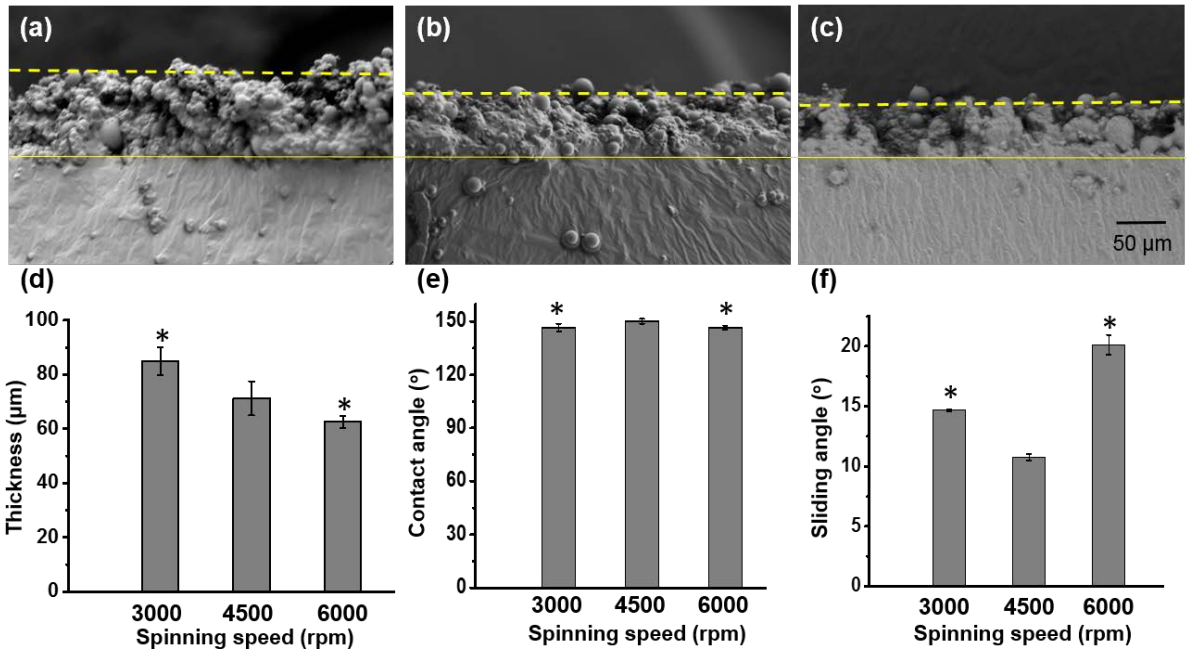

Fig. S6. Thickness of the upper silicone elastomer/silica microparticle layer under different spin-coating speeds and the wettability on the as-prepared surfaces. (a-c) SEM images of the superhydrophobic surfaces at spin-coating speeds at 3000, 4500, and 6000 rpm, respectively. The cross-sectional views indicated a decreasing thickness of the elastomer coating with increasing spin-coating speed. (d) The thickness of the composite coating decreased from approximately 80 μm at 3000 rpm to 70 μm at 4500 rpm and 60 μm at 6000 rpm. (e) With spin-coating speed increasing from 3000 to 6000 rpm, the water contact angles on the surfaces maintained above 150°. (f) Using 8 μL of water droplet, the surface prepared at 4500 rpm exhibited the lowest sliding angle. *$P<0.05$, comparable to the group with spin-coating speed at 4500 rpm.

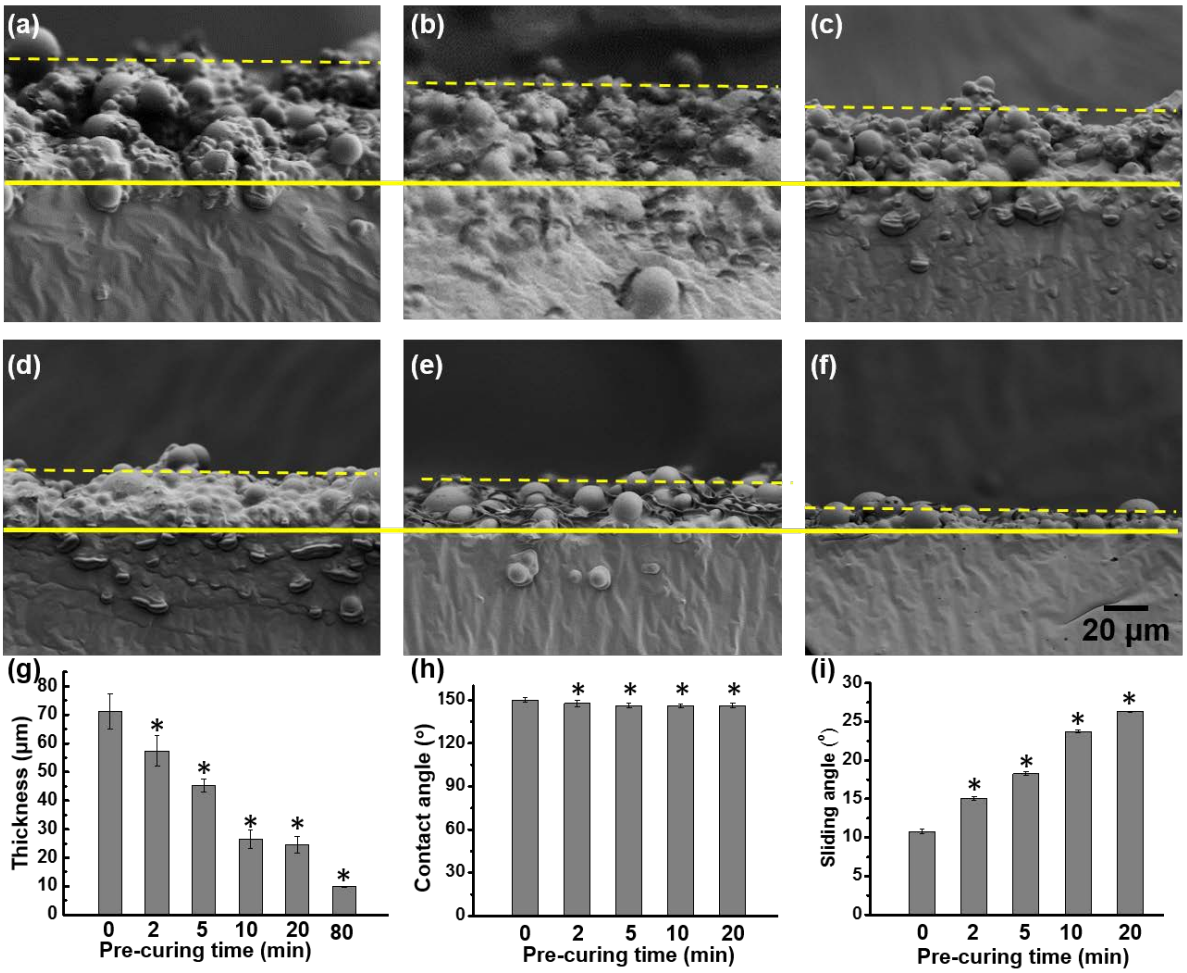

Fig. S7. Thickness of the upper silicone elastomer/silica microparticle layer under different pre-curing time and the wettability on the as-prepared surfaces. (a-f) The cross-sectional views of SEM images of superhydrophobic surfaces prepared with pre-curing time 0 min, 2 min, 5 min, 10 min, 20 min, and 80 min before depositing silica particles. (g) With prolonged pre-curing time, the thickness of the upper elastomer/silica microparticle composite layer decreased accordingly. (h) The surfaces prepared under different pre-curing times gave the similar water contact angles, around 150°. (i) The sliding angle increased with prolonged pre-curing time. *P<0.05, comparable to the group with pre-curing time of 0 min.

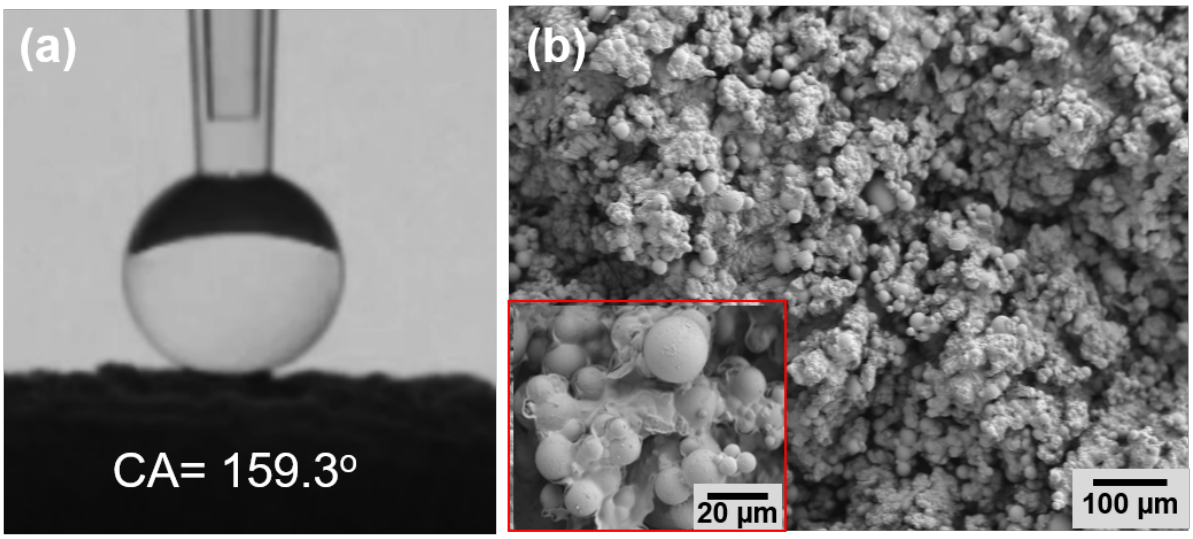

Fig. S8. (a) Water droplet sitting on a superhydrophobic elastomer under a strain of 500%. (b) SEM image showing the microstructures of the superhydrophobic surface after it broke beyond a strain of 500% and relaxed. The inset is a magnified view.

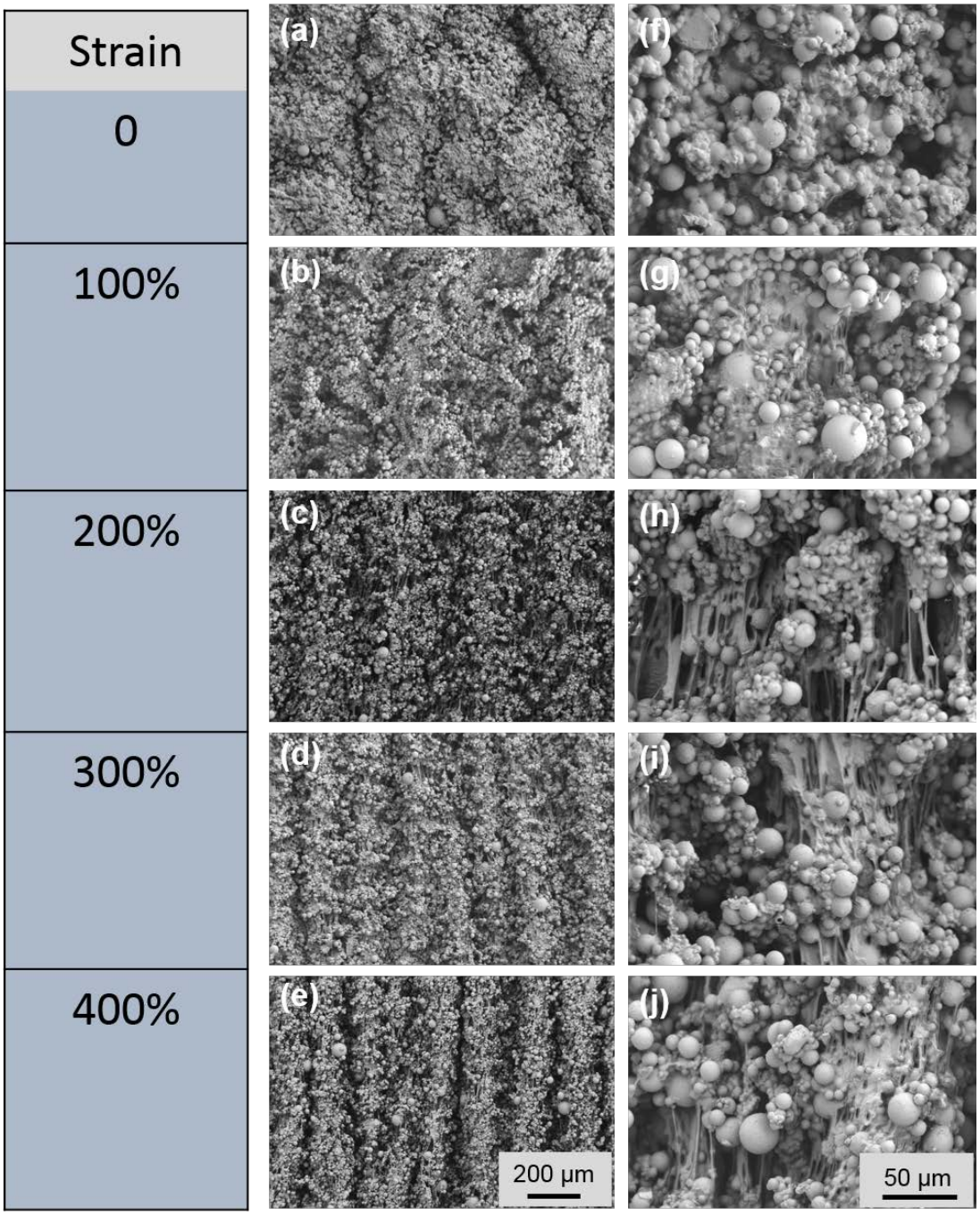

Fig. S9. Evolution of anisotropic microstructures with increasing strain; values in the left most column indicate the corresponding strain in the row. (a-e) SEM images of the superhydrophobic surfaces with uniaxial tensile strains of 0, 100%, 200%, 300%, and 400%, showing appearance of increasingly evident grooves and anisotropy. (f-j) Magnified images corresponding to (a-e), respectively.

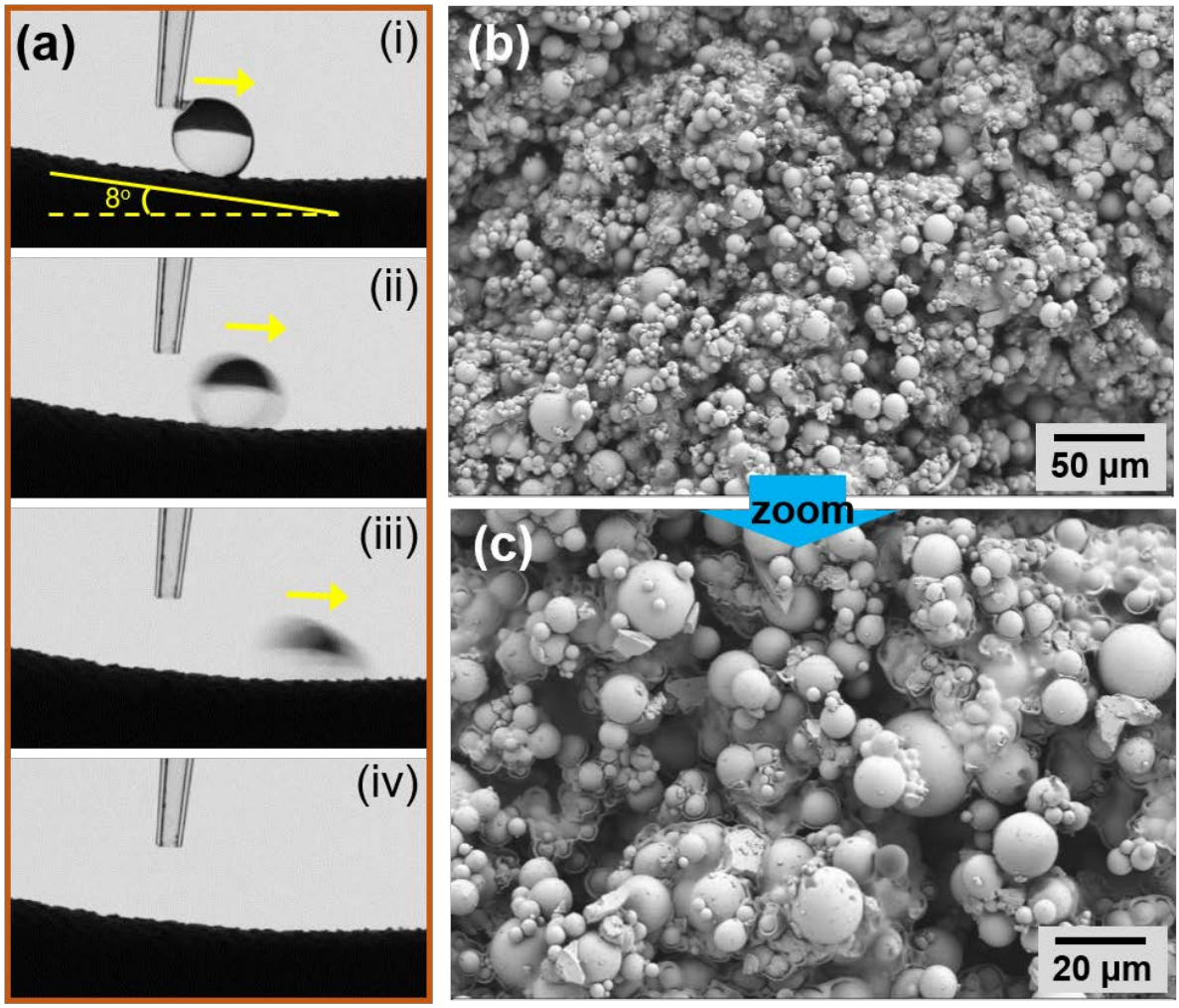

Fig. S10. Wettability and microstructure of superhydrophobic elastomer after repeated stretching and relaxing for 1000 cycles. (a) A water droplet of 8 μL can slide off the surface with a tilt angle of 8°. (b-c) SEM images of the superhydrophobic surface after 1000 cycles of stretching-relaxing treatment.

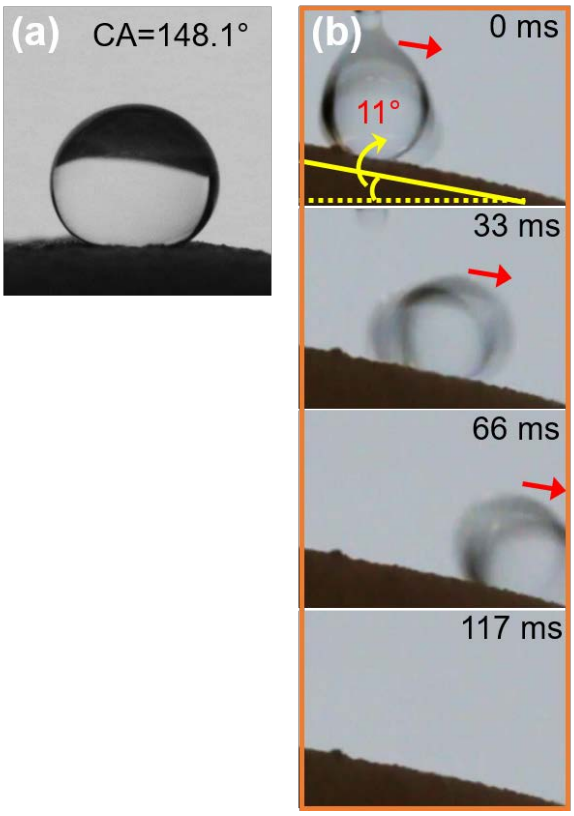

Fig. S11. (a) Water contact angle and (b) sliding angle of the superhydrophobic surface after severe rubbing process. Water contact angle was obtained by placing a water droplet of 5 µL gently on the surface; sliding angle was obtained by placing a water droplet of 8 µL on the surface and then tilting the surface slowly until water droplet started to move.

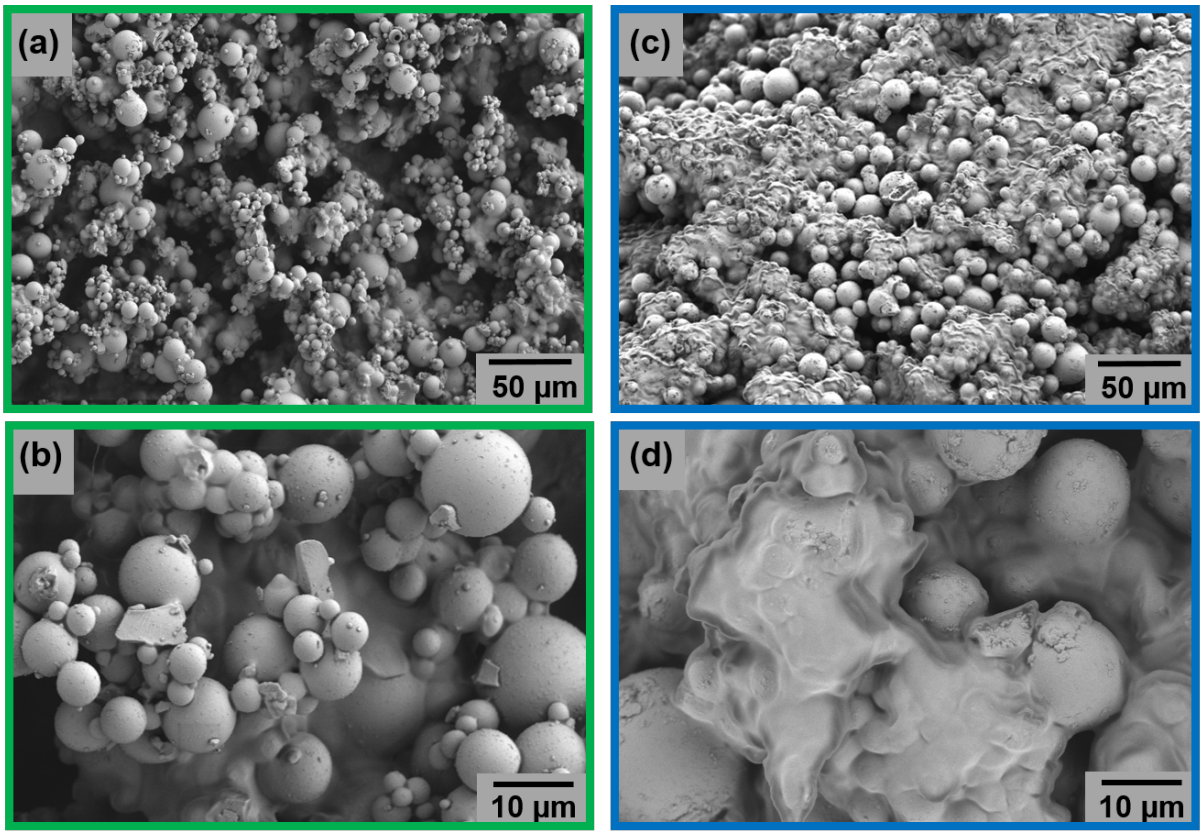

Fig. S12. SEM images of the superhydrophobic surface without chemical bonding before and after the rubbing process. (a) and (b) Before rubbing, the silica microparticles were distributing densely on the surface. (c) and (d) After rubbing, many silica microparticles were exfoliated, leaving large areas of bare silicone elastomer without coverage by silica microparticles. (b) and (d) are magnified images of (a) and (c), respectively.

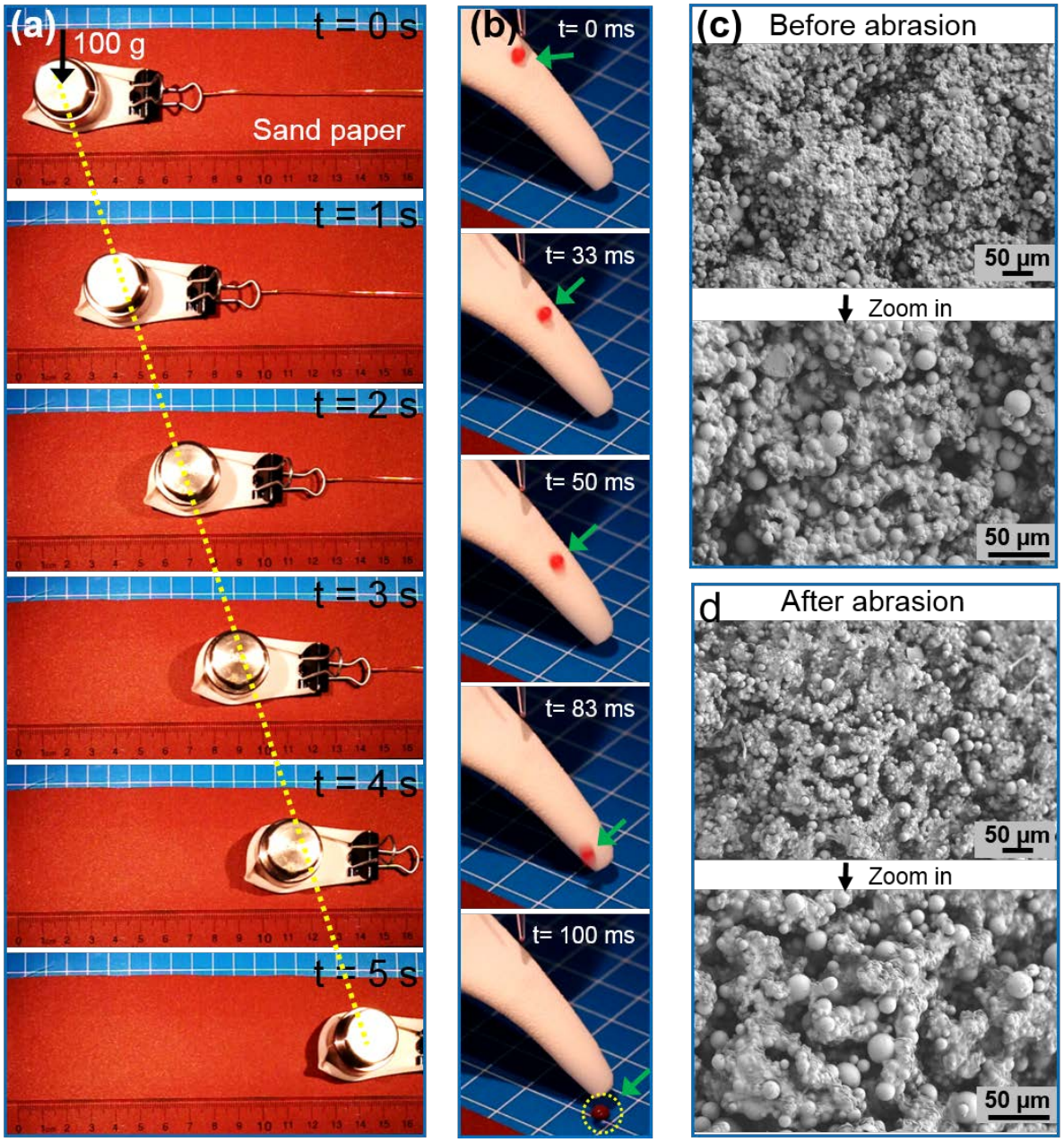

Fig. S13. Abrasion test of the superhydrophobic surface. (a) The superhydrophobic surface pressed against a 500-grit sandpaper surface under a 100-g weight was made to move horizontally for about 12 cm within 5 s. (b) After the abrasion treatment, the superhydrophobic surface maintained repellence to water droplet. (c) and (d) SEM images of the superhydrophobic surfaces before and after sandpaper abrasion test, showing negligible difference.

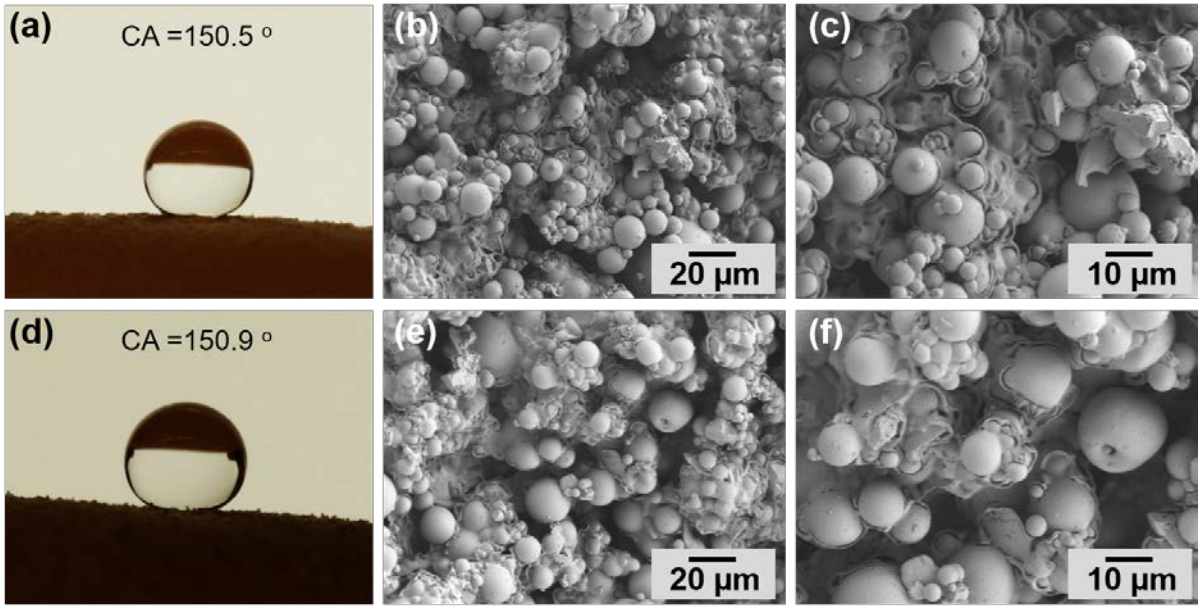

Fig. S14. Water contact angles and SEM images of the superhydrophobic surface after (a-c) 5 and (d-f) 10 cycles of sandpaper abrasion cycles.

Movie S1. An 8-μL water droplet moving fluently down off the inclined superhydrophobic surface at strain = 0%.

Movie S2. An 8-μL water droplet moving fluently down off the inclined superhydrophobic surface at strain = 200%.

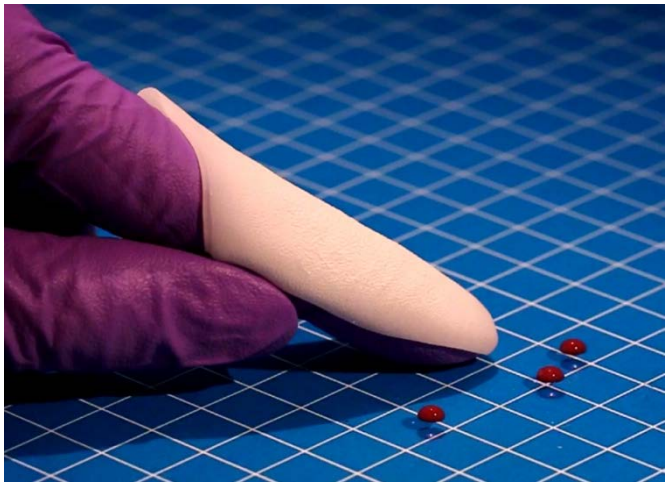

Movie S3. Robustness of the superhydrophobic surface after the rubbing process.